

## Supporting information

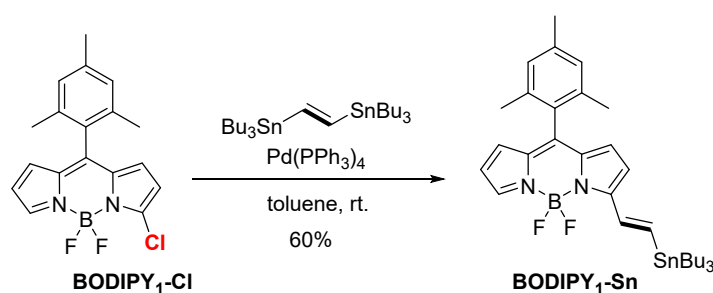
### A PEGylated conjugated-BODIPY oligomer for NIR-II imaging-guided photothermal therapy

Yuan Wang<sup>†</sup>, Tongtong Shan<sup>†</sup>, Jiahao Zheng, Jia Tian, Weian Zhang<sup>\*</sup>

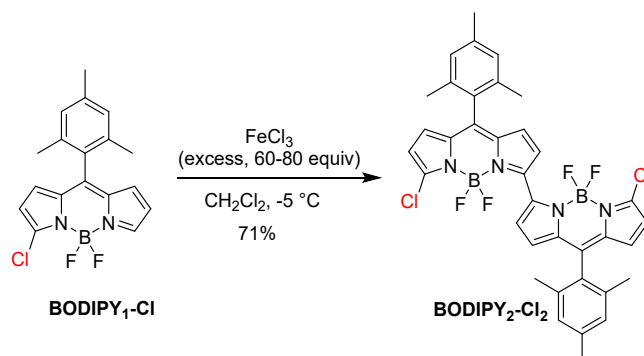
Shanghai Key Laboratory of Functional Materials Chemistry, East China University of Science and Technology, Shanghai 200237, China.

**\*Corresponding Authors:** [wazhang@ecust.edu.cn](mailto:wazhang@ecust.edu.cn)

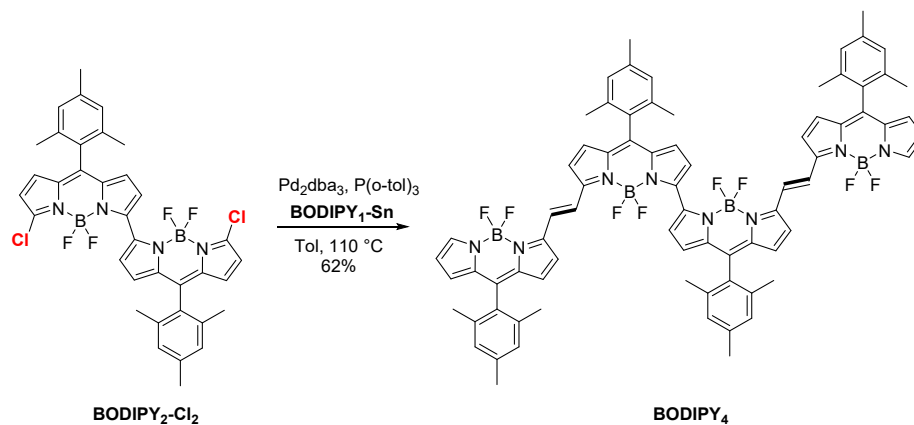
<sup>†</sup>Yuan Wang, Tongtong Shan contributed equally to this work.



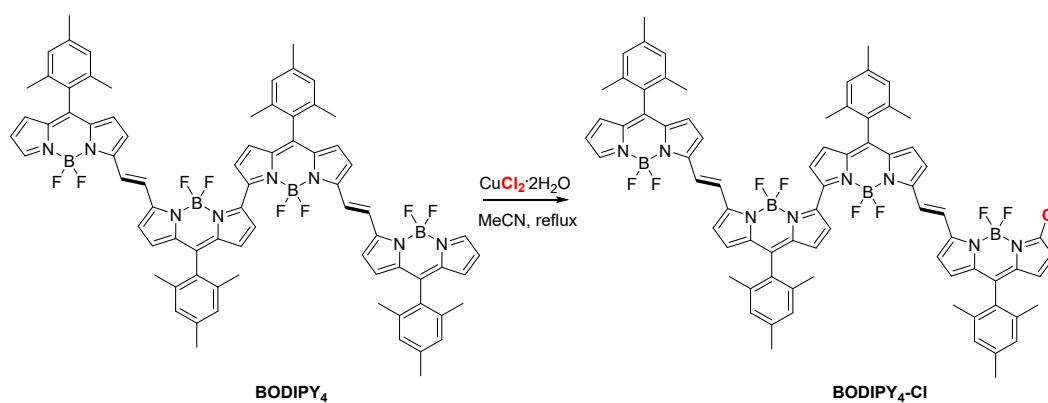
**Scheme S1.** Synthesis of BODIPY<sub>1</sub>-Sn.



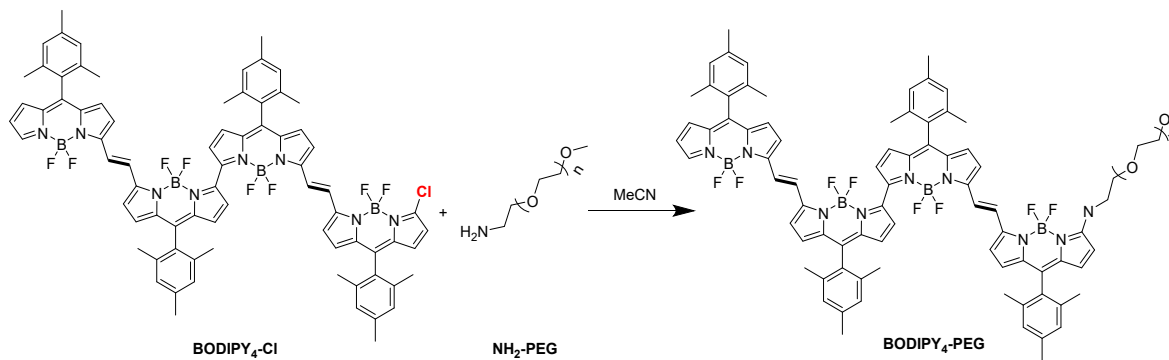
**Scheme S2.** Synthesis of BODIPY<sub>2</sub>-Cl<sub>2</sub>.



**Scheme S3.** Synthesis of BODIPY<sub>4</sub>.



**Scheme S4.** Synthesis of BODIPY<sub>4</sub>-Cl.



**Scheme S5.** Synthesis of BODIPY<sub>4</sub>-PEG.

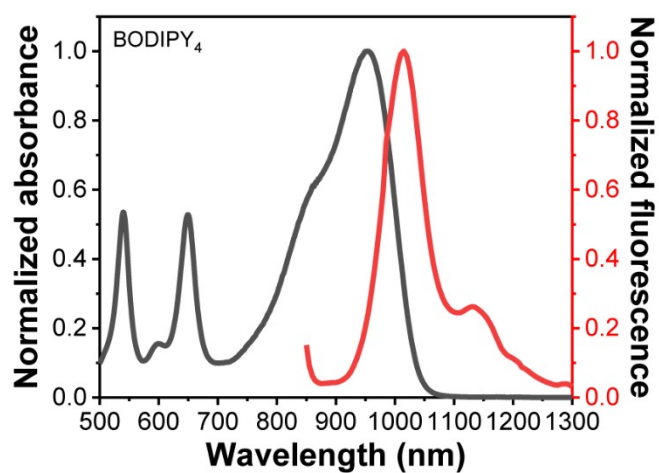


**Fig. S1.** Absorbance and emission spectra of BODIPY<sub>4</sub>.

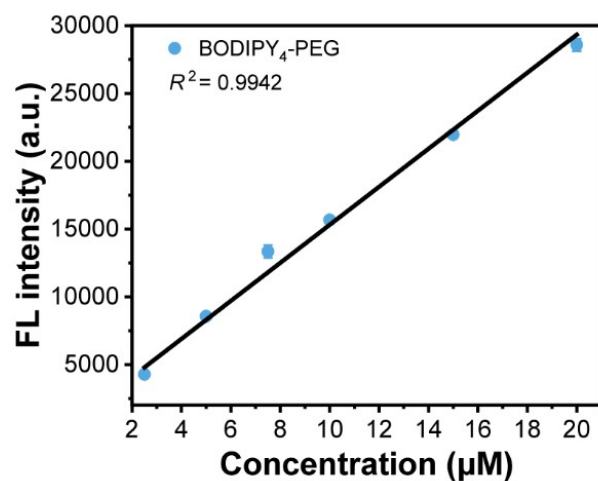


**Fig. S2.** The linear relationship between concentration and fluorescence intensity of BODIPY<sub>4</sub>-PEG.

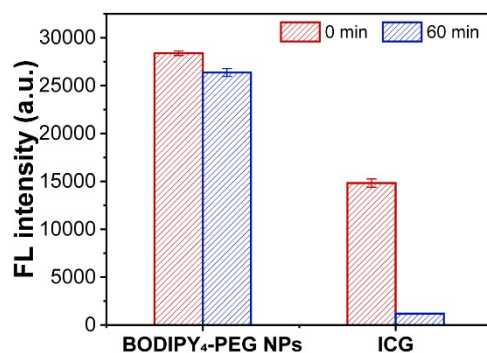


**Fig. S3.** Photostability of BODIPY<sub>4</sub>-PEG and ICG.

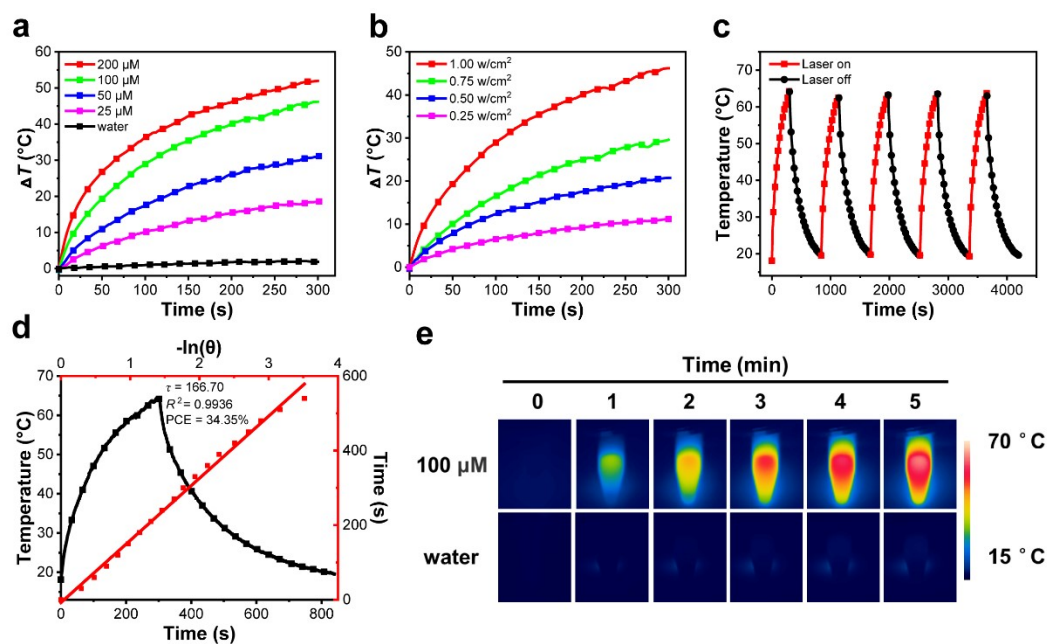


**Fig. S4.** Photothermal conversion curves of BODIPY<sub>4</sub>-PEG NPs aqueous solution at various concentrations (a) and different power densities (b) (100 μM) under 808 nm laser irradiation for 5 min. (c) Photothermal stability of BODIPY<sub>4</sub>-PEG. The heating and cooling cyclic curves of BODIPY<sub>4</sub>-PEG (100 μM) under 808 nm laser irradiation (1.00 W cm<sup>-2</sup>, 5 cycles). (d) The heating-cooling curve of BODIPY<sub>4</sub>-PEG aqueous solution (100 μM) under 808 nm laser irradiation (1.00 W cm<sup>-2</sup>) (heating time 5 min, cooling time 9 min) and the relationship between  $-\ln(\theta)$  and cooling time calculated by the curve and formula. (e) Thermal images of BODIPY<sub>4</sub>-PEG and water under 808 nm laser irradiation (1.00 W cm<sup>-2</sup>, 5 min).

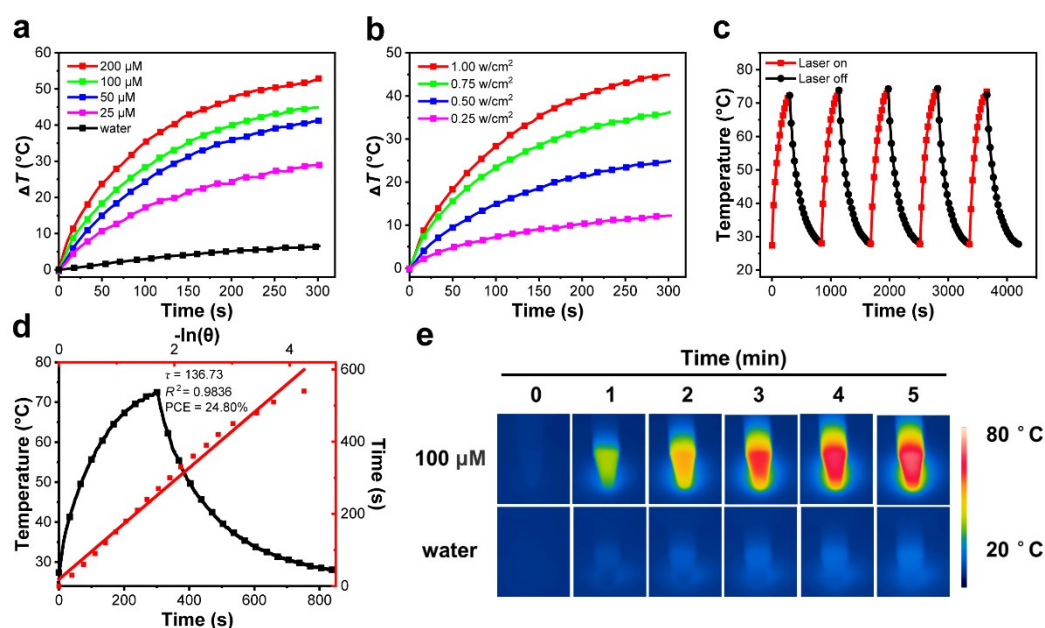


**Fig. S5.** Photothermal conversion curves of BODIPY<sub>4</sub>-PEG NPs aqueous solution at various concentrations (a) and different power densities (b) (100  $\mu\text{M}$ ) under 1064 nm laser irradiation for 5 min. (c) Photothermal stability of BODIPY<sub>4</sub>-PEG. The heating and cooling cyclic curves of BODIPY<sub>4</sub>-PEG (100  $\mu\text{M}$ ) under 1064 nm laser irradiation (1.00  $\text{W}/\text{cm}^2$ , 5 cycles). (d) The heating-cooling curve of BODIPY<sub>4</sub>-PEG aqueous solution (100  $\mu\text{M}$ ) under 1064 nm laser irradiation (1.00  $\text{W}/\text{cm}^2$ ) (heating time 5 min, cooling time 9 min) and the relationship between  $-\ln(\theta)$  and cooling time calculated by the curve and formula. (e) Thermal images of BODIPY<sub>4</sub>-PEG NPs and water under 1064 nm laser irradiation (1.00  $\text{W}/\text{cm}^2$ , 5 min).

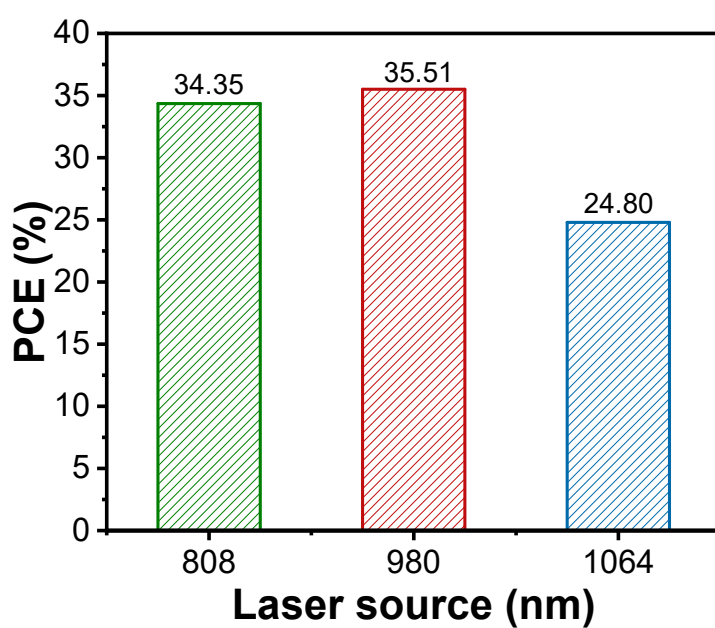


**Fig. S6.** Summary of PCEs of BODIPY<sub>4</sub>-PEG under different laser sources.

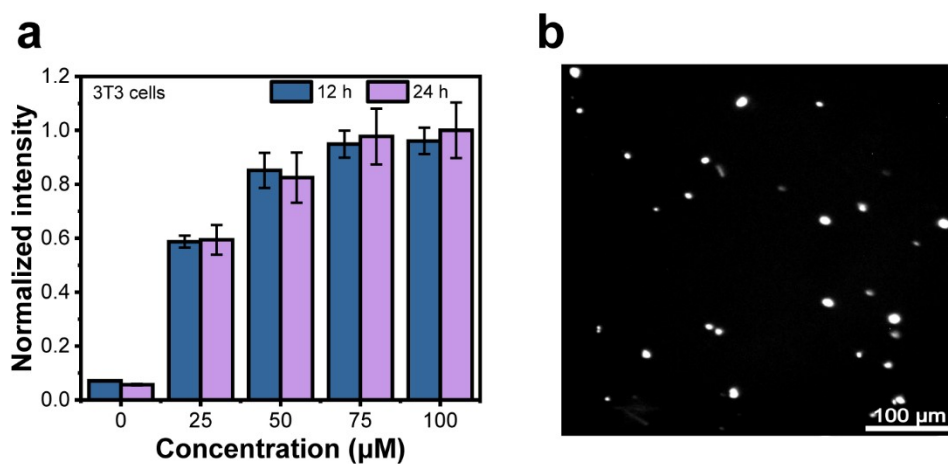


**Fig. S7.** (a) Quantitative statistic of 3T3 cells' uptake intensity after coincubation with BODIPY<sub>4</sub>-PEG for 12 h or 24 h. (c) Photograph of 4T1 cells after co-incubating with BODIPY<sub>4</sub>-PEG for 24 h (808 nm, 1000 LP, 1000 ms).

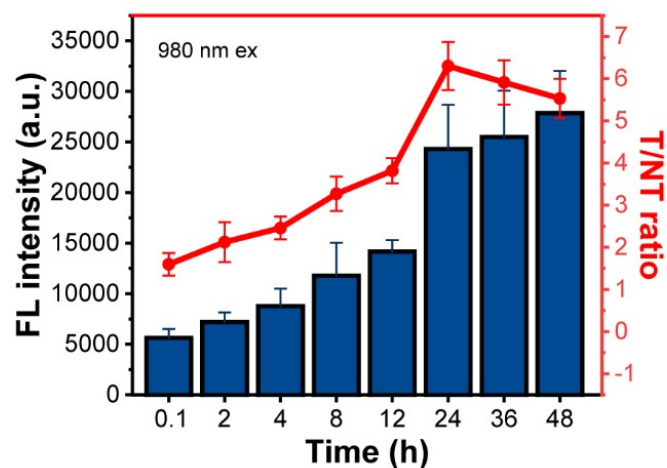


**Fig. S8.** Quantitative statistics of fluorescence intensity at 4T1 tumor sites.

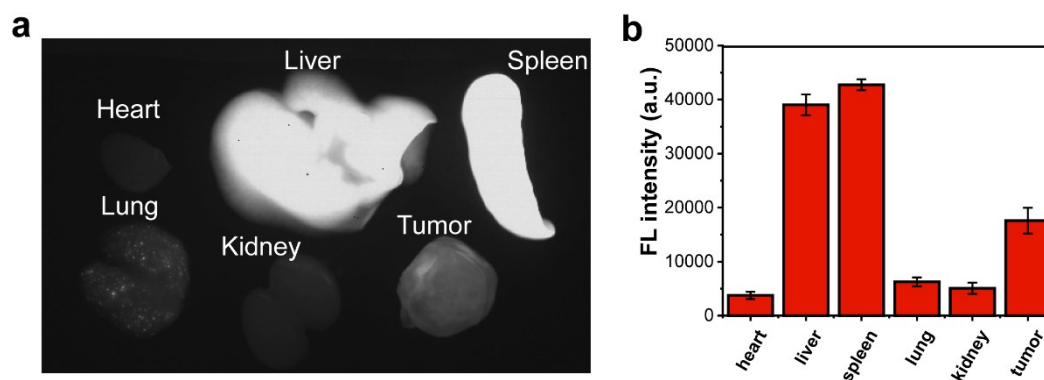


**Fig. S9.** (a) NIR-II fluorescence image of major organs and tumor resected at 48 h post-injection of BODIPY<sub>4</sub>-PEG. (d) Quantitative statistics of fluorescence intensity of major organs and tumors (n = 3).

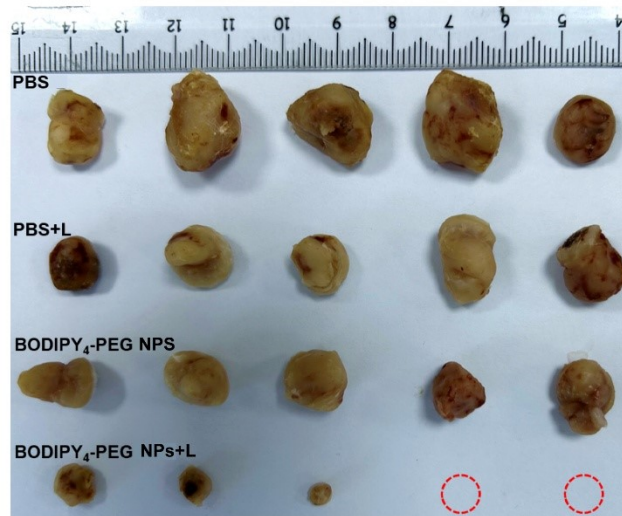


**Fig. S10.** Photographs of the 4T1 tumors excised from the mice after the four treatments with PBS, PBS+L, BODIPY<sub>4</sub>-PEG NPs, and BODIPY<sub>4</sub>-PEG NPs+L as indicated.

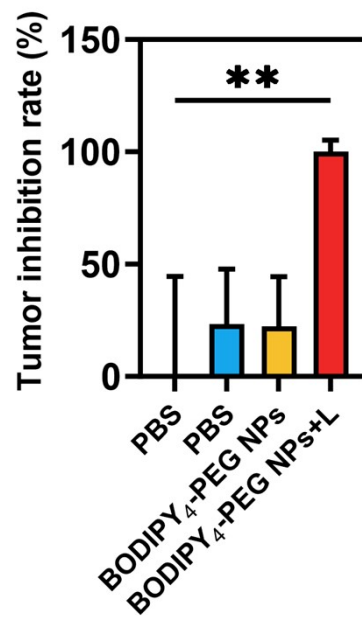


**Fig. S11.** Curves of tumor inhibition rates for different experimental groups (n = 5, mean  $\pm$  SEM) and n represented independent experiments. \*\*P < 0.01.



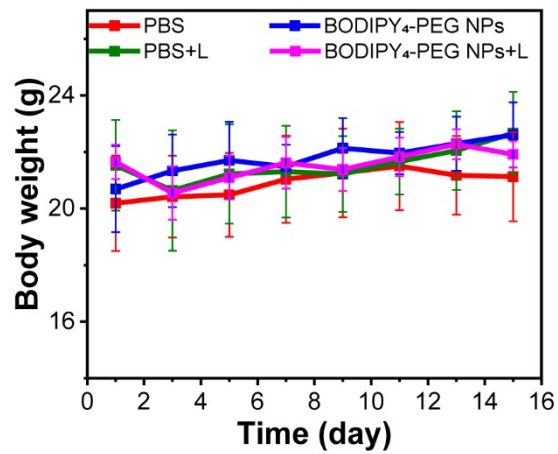


**Fig. S12.** Variation curve of body weights of mice under the four treatments (n = 5, mean  $\pm$  SEM).

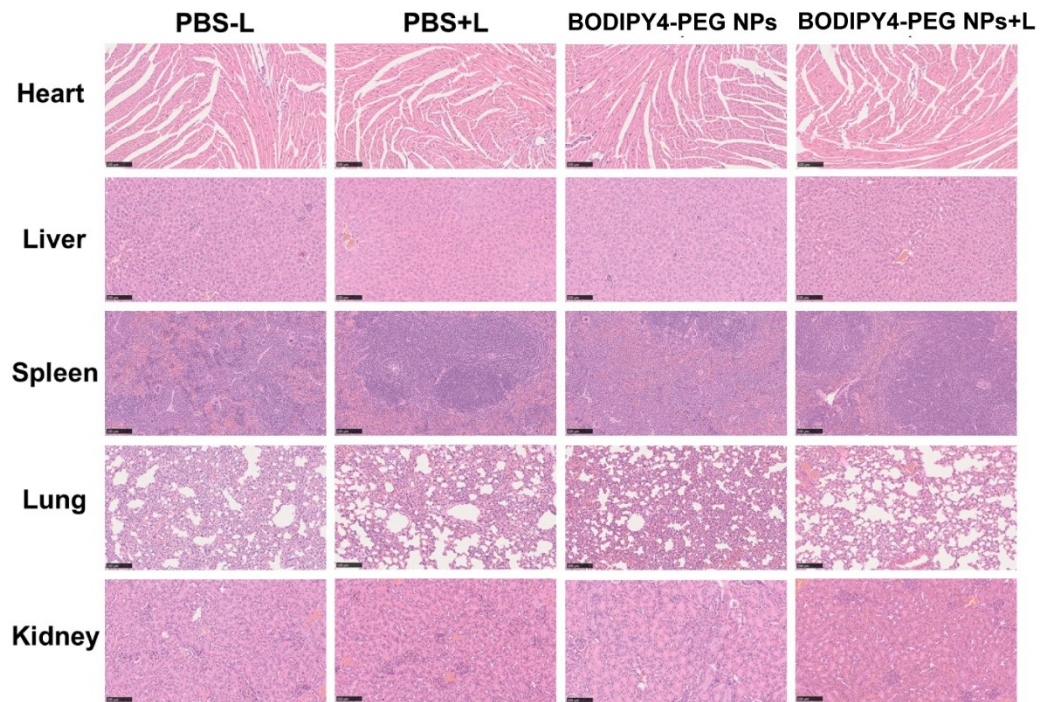


**Fig. S13.** H&E staining images of the main organs including the heart, liver, spleen, lung, and kidney of mice in different treatment groups. Scale bar: 100  $\mu$ m.

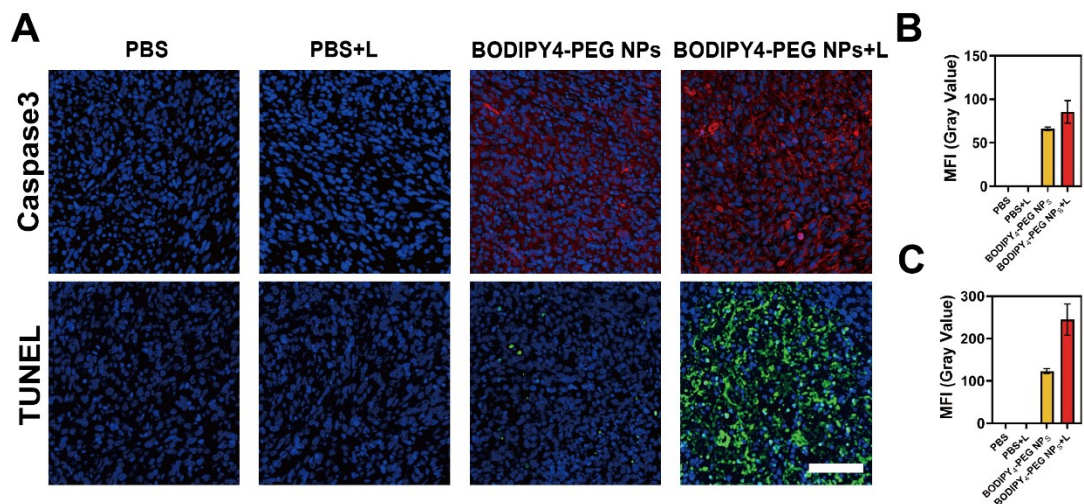


**Fig. S14.** Immunofluorescence staining experiments. (A) The staining results of Caspase-3 and TUNEL, as well as the quantification of their fluorescence intensities (B) and (C). Scale bar: 100  $\mu\text{m}$ .

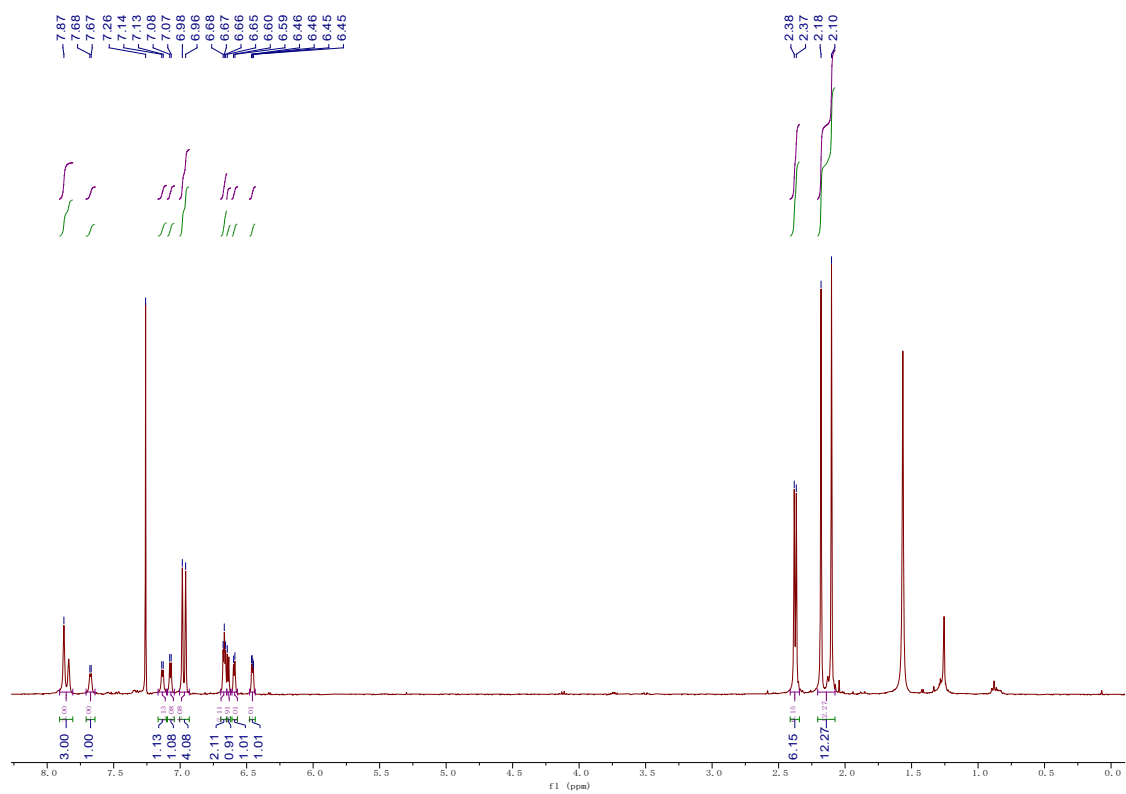


**Fig. S15.**  $^1\text{H}$  NMR spectrum of BODIPY<sub>4</sub> in  $\text{CDCl}_3$ .

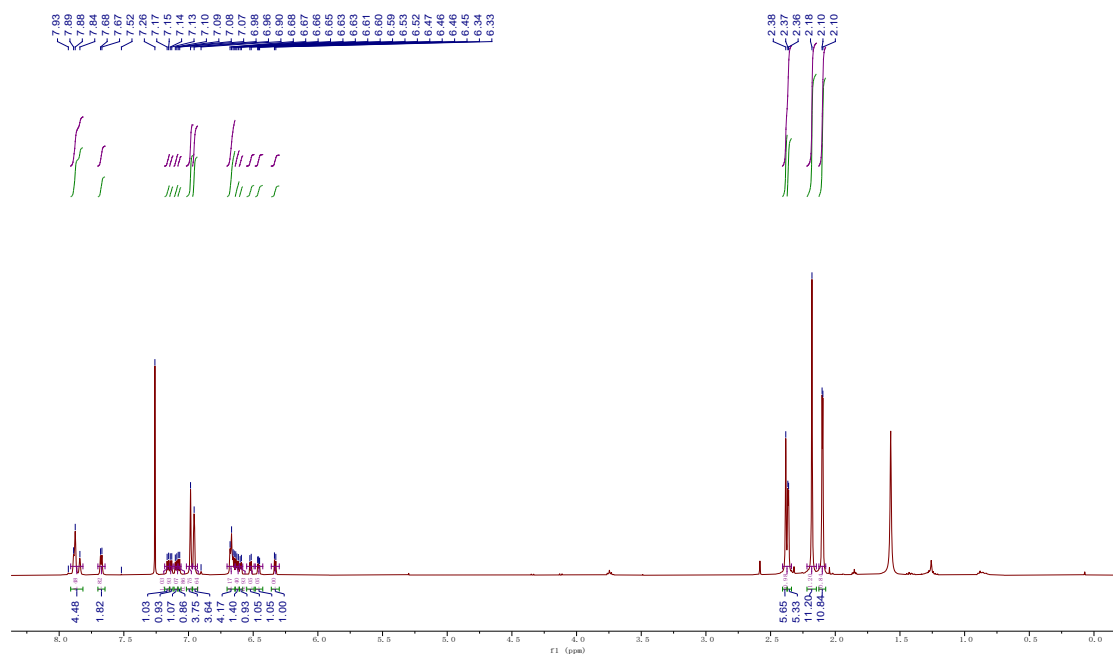


**Fig. S16.**  $^1\text{H}$  NMR spectrum of BODIPY<sub>4</sub>-Cl in  $\text{CDCl}_3$ .

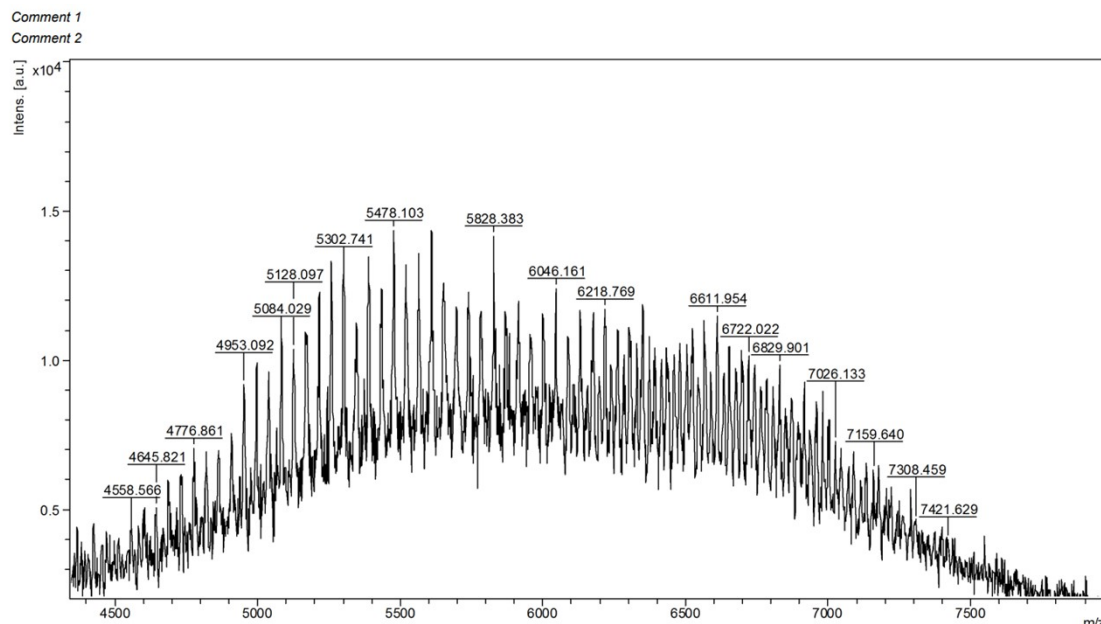


**Fig. S17.** The MALDI-TOF-MS of BODIPY<sub>4</sub>-PEG.